49th Canadian Geotechnical Conference
of the Canadian Geotechnical Society
23-25 September 1996, St. John's, Newfoundland

MODELLING FIRST-YEAR ICE RIDGE KEELS WITH SAND

Stephen E. Bruneau
C-CORE, Memorial University of Newfoundland, Canada, A1B 3X5

ABSTRACT

When a first-year sea ice ridge interacts with an offshore structure, loads are created by the breaking of refrozen ice in the ridge core and the clearing of the above- and below-water portion of the rubble accumulation (sail and keel). In an effort to improve ridge keel load modelling, experiments have been conducted using piles of dry sand that model, in inverted form, a granular ice keel. Though no scaling of loads is intended, the "sand keel" approach sheds light on fundamental failure mechanisms for the indentation of keel-like accumulations of a granular material. A load model is developed for sand which provides a basis for an analytical model for full-scale ridge keels. The ease and simplicity of systematic testing with sand is in sharp contrast to experimenting with floating ice rubble in the lab. Moreover, parametric studies on ice rubble in the field is prohibitively expensive and difficult owing to the scale and prevailing environmental conditions of natural ridges.

RÉSUMÉ

Lorsqu'un amoncellement de glace de mer de première année est en contact avec une structure marine, les forces sont dues au broyage de la glace recongelée au centre du monticule et au dégagement au-dessus et sous la surface de l'eau de l'amoncellement de blocs (voile et quille). En vue d'améliorer la modélisation du chargement exercé par la quille de l'amoncellement, des essais ont été effectués avec des tas de sable sec qui simulaient, sous une forme renversée, une quille de glace granulaire. Cette approche n'aspire pas à reproduire l'échelle réelle du chargement. Elle contribue cependant à clarifier les mécanismes fondamentaux de rupture par indentation dans des amas de matériau granulaire ayant la forme d'une quille. Pour le sable, on présente un modèle de chargement servant de base pour l'élaboration d'un modèle analytique simulant une quille de crête grandeur nature. La facilité et la simplicité de cette approche contraste fortement avec l'expérimentation en laboratoire ayant recours à des monticules de glace flottante. De plus, la dimension et les conditions environmentales dominantes des amoncellements naturels rendent coûteuses et difficiles les études paramétriques des accumulations de glace sur le terrain.

INTRODUCTION

First-year compression ridges usually form at the boundary of two ice sheets or spontaneously within an ice sheet due to excessive compressive stresses early in the winter season. The crushing and fracturing of the ice sheet produce blocks and brash that are ultimately forced beneath the surface forming the *keel* and to a lesser extent are forced upward to form the *sail* of a ridge. In time, the keel becomes interlocked with a refrozen core that forms at the waterline and may exceed parent ice thickness. When conditions cause laterally extensive accumulations *rubble fields* are produced. If formed to a sufficient size (e.g. 15+ m depth, 1 m block length) first-year compression ridges may present the design loads for subarctic offshore structures making studies of their mechanical properties an important design issue.

Typically keel shape is assumed to be triangular in cross-section with an average slope between 28° and 32° though it can be shown (Bruneau, 1996) that this approximation underestimates the sectional area by about 12% on average. A half-sine (continuous wave form) with similar maximum width and depth dimensions provides a better approximation. A trapezoid is better for estimating wide ridges and rubble fields though additional information is required and slope discontinuities, which can be a problem analytically, remain. Keel ice rubble creeps and bonds according to contact duration, pressure and temperature. These conditions, and the salinity of pore fluid, block size and bulk porosity, affect the bulk shearing resistance. In the lab when floating ice rubble is newly formed, relatively warm and is sheared quickly, it behaves like a cohesionless soil (at least at pressures below 20 kPa). If pressure and heat conduction cause freeze bonding then ice rubble may possess cohesive properties. The *cohesion* is time-dependant however, and is not lost indefinitely after being disturbed. Bonds reform quickly under pressure and, due to creep, may not fracture with slow relative movement between blocks.

Figure 1 is a plot of laboratory ice rubble shear data collected from the literature. The theoretical behaviour of a loose and dense sand, plastic blocks and solid ice is shown for reference. The lower bound strength (or weakest state) of ice rubble undergoing shear is similar to that of loose sand. The scatter in the upper portion is attributable to various degrees of inter-block bonding. It is conjectured that the plastic deformation of "sand keels" in the lab may provide a simplistic but effective analogue for natural ridge failure processes. Scaling of forces is not intended. The absence of cohesion in sand tests is not expected to adversely influence the applicability of experimental results. In the study of soil failure in front of tines it has been observed that rupture distance (leading extent of failure pattern) is substantially independent of cohesion (Osman, 1964) and moisture content in sand (Rajaram and Oida, 1992).

EXPERIMENTAL PROGRAM

The force required to break through a discrete sand pile may be considerably less than that for steady-state ploughing conditions in a level sand layer. Also the indentation of keels is more complicated than passive pressure on retaining walls because a non-linear, transient surcharge develops and clearing processes are activated. Thus earth pressure and draught formulae in geotechnical and agricultural engineering practice are limited in their application to keel

interactions. As a result the following topics were identified for study: the sensitivity of indentation force and penetration to keel and structural shape, the influence of structure width on the failure loads, and the evolution of load and failure patterns with penetration into continuous sand layers.

Experiments were performed at C-CORE, Memorial University of Newfoundland. All experiments were conducted with silica sand Type 0. A 1 m square tank approximately 0.75 m deep was used to contain the sand and support a mechanical drive arm for horizontally translating plastic model structures (Figure 2). The models were vertically supported by two cantilever load cells and, when translated, maintained a constant clearance of 4 mm with a sandpaper-covered false floor. All tests were conducted at 6 mm/s. Sand formations were constructed by placing piles of loose sand across the tank floor in front of a model structure. Precise shaping was achieved using plywood trowels cut out to the required cross-sectional shape which, when dragged over the loose piles, created the desired prismatic keel form. Where a continuous layer of sand was required flat trowelling and a depth gauge were used. Sand was mixed and consistently replaced before each experiment to maintain a consistent density.

For structures indenting symmetrical trapezoid keel formations dimensional analysis yields:

$$\frac{F}{\gamma H^2 D} = f\left(\alpha,\ \delta,\ \phi_1,\ \phi,\ \frac{W}{D},\ \frac{H}{D},\ \frac{P}{D}\right) \qquad [1]$$

where **F** is horizontal force, γ is bulk weight (13880 N/m^3 for sand tested), α is the slope of the structure, δ is soil surface slope, ϕ_1 is the soil-structure friction angle (0.6ϕ for sand and plastic), ϕ is the angle of internal friction ($\approx 32°$ for loose sand tested), **W** and **H** are the "sand keel" width and depth, **D** is the structure projected width and **P** is structure penetration from the sand keel leading edge. For tines indenting soil there is a critical depth aspect ratio (rubble depth to structure width) above which material is displaced forwards, sideways and upwards, and below which no upward movement occurs. Reported values for the critical depth aspect ratio are widely varied with a median value around 7 (Godwin and Spoor, 1977). This study is aimed at applications where aspect ratio is typically no greater than 3, remaining above the critical depth.

Experimental Results

Figure 3 illustrates the relative influence of sand keel shape on peak load and penetration at peak. All five keels (shown beneath the bar graph) had the same sectional area and two different widths were used. Loads were normalized against the 320 mm-wide trapezoid sand keel because it resulted in the highest load and was also the preferred default shape in subsequent tests. Generally, the wider shorter keels resulted in lower loads and significantly greater penetrations at peak. There was little difference between the loads on keels of similar width.

Figures 4 and 6 illustrate the influence of structural shape on peak indentation force for both trapezoidal sand keels and for a continuous sand layer (steady-state loading achieved). Each

model shape (shown in Figure 4) had the same projected frontal width. The load on the circular cylinder was used to normalize loads for the trapezoidal indentation tests and the square section was similarly used for the continuous layer tests because each produced the respective maxima. The results which show little variation for trapezoidal indentation and moderate differences for continuous layer indentation are in stark contrast to the substantial variation in drag of similar two dimensional bodies in a fluid.

To establish the quantity of load attributable to "edge effects" flat vertical structures of width **D**, **2D**, and **3D** were translated through sand keels. Peak indentation force for each test was normalized against that for the structure of width **D** (Figure 5). By extrapolating to the normalized force intercept, one obtains a force at an effective width of zero. In this study the edge effect force was 50% of the total indentation force for the structure of width **D** where the keel was 2.8**D** wide and 2/3**D** deep. Thus, the *effective* width of the structure, $\mathbf{D_{eff}}$, was **D**(1+1.5**H/D**). Sample force traces for the three widths are plotted in Figure 6.

The relative penetration to peak load has been determined for a range of **W/D** and **H/D** ratios for vertical cylinders indenting trapezoidal sand keels (Figure 7). Multiple regression techniques were applied to determine the expression shown which has a goodness-of-fit adjusted r^2 value of 97%. Lastly, continuous sand layers were indented until steady state conditions arose. The point at which steady state failure occurred was approximated because it is a cyclic collapse mechanism (as described by Rajaram and Oida, 1992). Forward rupture distance, **r**, side rupture distance, **s**, surcharge height at the structure, $\mathbf{H_s}$, and horizontal force were measured at 5 cm penetration intervals for a range of **H/D** (Figure 8). Expressions for **r**, **s**, and $\mathbf{H_s}$ shown on the figure have been formulated using multiple regression techniques yielding, in all cases, adjusted r^2 values greater than 93%. Patterns of increase and stabilization are the same for all measured quantities. Measurements of **r** and **s** required some judgement since rupture form was slightly asymmetric at times and the cyclic formation of leading rupture edges meant that these dimensions ratchetted as the structure advanced.

DEVELOPMENT OF LOAD MODEL: Cylindrical Structures, Trapezoidal Keels

When a cylindrical structure penetrates a "sand keel", the sand accumulates in a raised crescent around the leading edge with the rupture distance extending further from the structure as surcharge deepens. The failure surface is rounded and cusp-like until shear planes, flaring from the structure to the back of the keel, form. Failure patterns were observed and sketched (Figure 6) from time lapsed photographs taken through a window with a model structure brushing past. For the trapezoidal sand keel in Figure 6, the failure surface extended upwards at a steep angle from position 0 through to some time after position 1. At that point a transition occurred whereby the sand within the main body of the pile ahead of the structure became fully mobilized. This transition in failure mode appears to mark the point where the classical local passive failure system collapses with the diminished confining stresses at the rear of the pile - promoting an outward instead of upward displacement of sand. In Figure 6 it can be seen that this transition between local and plug-like failure also marks the zone in which peak load occurs.

An algorithm for computing peak load requires modelling of only one of the failure modes described above because the point of incipient plug failure is known from the results in Figure 7. Thus, the well known passive earth pressure formula representing the local failure mode has been used and adapted for computing forces in this study as follows:

$$F = \frac{\gamma H_t^2 K_p D_{eff}}{2} \quad ; \quad K_p = \frac{\cos^2(\phi+\alpha)}{\cos^2\alpha\cos(\alpha-\phi_1)\left(1-\sqrt{\frac{\sin(\phi+\phi_1)\sin(\phi+\delta)}{\cos(\alpha-\phi_1)\cos(\alpha-\delta)}}\right)^2} \qquad [2]$$

where H_t is the total height of sand at the structure, D_{eff} is the effective width of the structure, and K_p is the effective passive pressure coefficient defined above in terms described earlier. The average surface slope, δ, was approximated as atan(H_t/2r) by observing in continuous layer indentation that overburden was approximately level over half of the rupture distance before sloping to the toe of the surcharge pile.

Indentation force has been computed as a function of penetration using two approximations for effective width, D_{eff} (Figure 8(d)). The first, method *A*, is $D(1+3H/2D) \leq 2D$ from above. Method *B* is an attempt to reconcile the computational procedure with observed failure shape. During local failure the cusp-like wedge of mobilized sand appears to have a uniform vertical cross-section (Figure 8). The whole body can thus be approximated geometrically by sweeping a vertical wedge of unit width circumferentially at either side of the cylinder projected width. The effective structural width, determined using this approximation, is:

$$D_{eff} = D + r\sin(\beta) \quad ; \quad \beta = atan(s/r) \qquad [3]$$

Measured forces are modelled slightly better by method *A* though both approximations are reasonably sound. The peak indentation load for any trapezoidal "sand keel" is obtained from Figure 8(d) by determining the penetration at peak for **H/D** and **W/D** from Figure 7.

CONCLUSIONS

A model of the indentation process for structures indenting "sand keels" has been successfully developed and tested. The procedure, based on passive earth pressure, provides a framework for full scale ridge keel modelling. Consideration of inertia and the effects of compressibility, pore pressure and boundary compliancy will further enhance modelling efforts. With additional testing semi-empirical relations for **r**, **s**, and H_s may be found for sloping structures including some cones. Similar analytical solutions are possible since with increased slope angle conical structures approach cylindrical form. For sloping structures in the ocean the waterline is likely to pass through the rubble bearing on the structure so that a discontinuity in the confining stress gradient exists. Once the boundary between upward and downward rubble failure and effective rubble weight have been determined, the modelling procedure above may be applied.

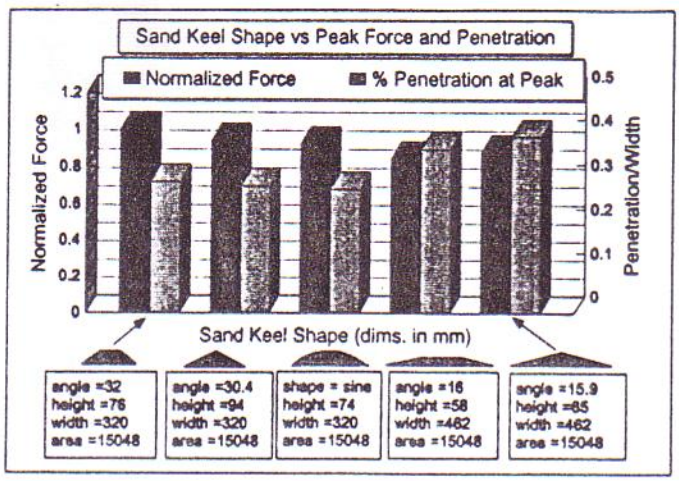

FIGURE 3.

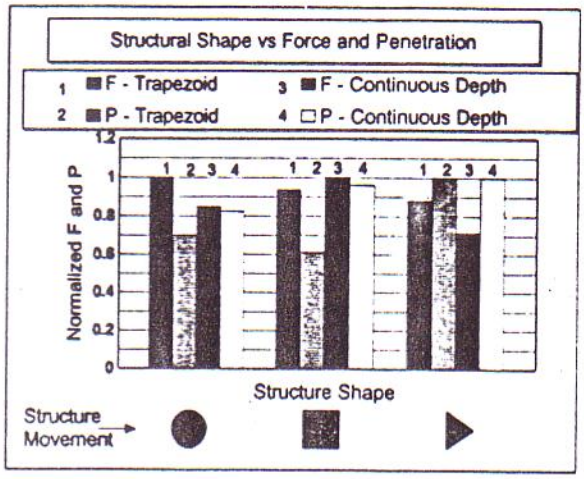

FIGURE 4.

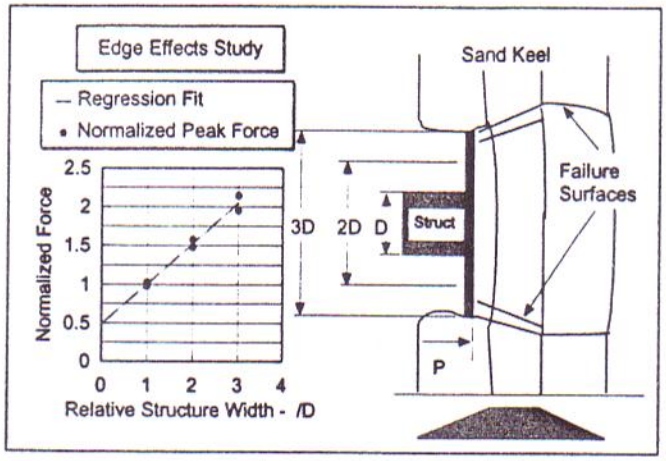

FIGURE 5.

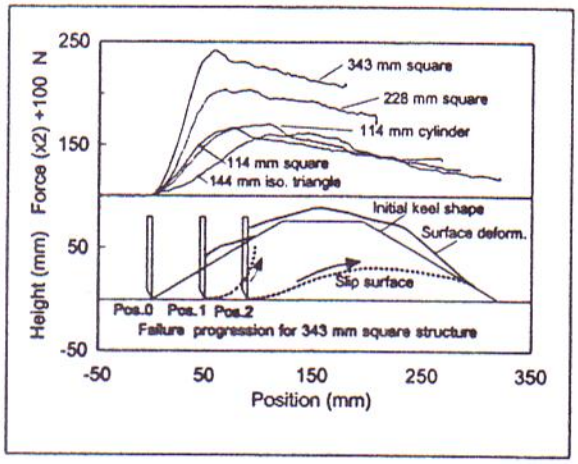

FIGURE 6.

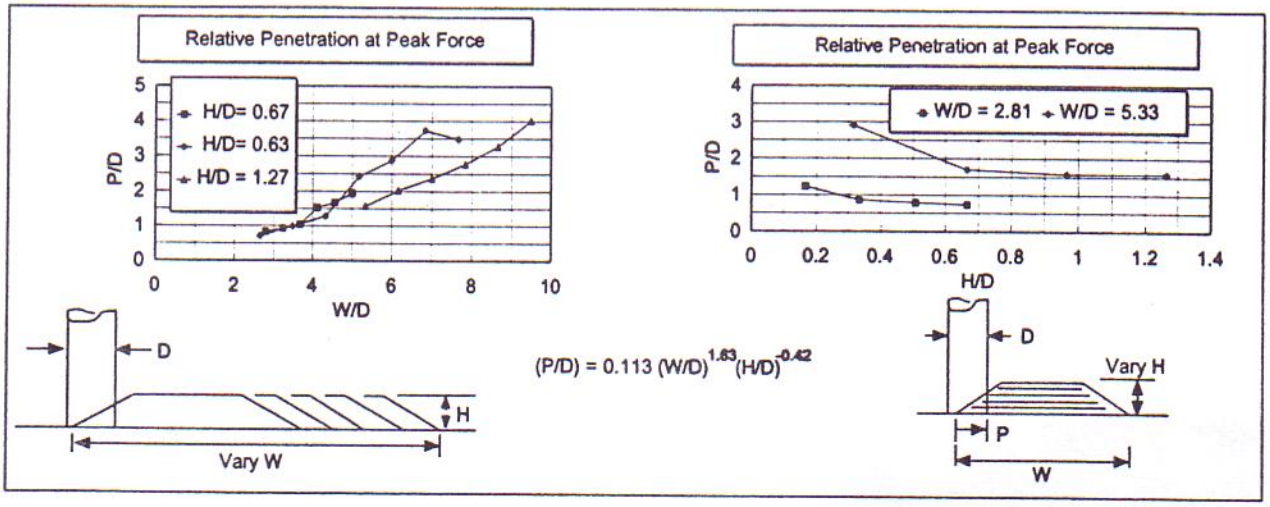

FIGURE 7.

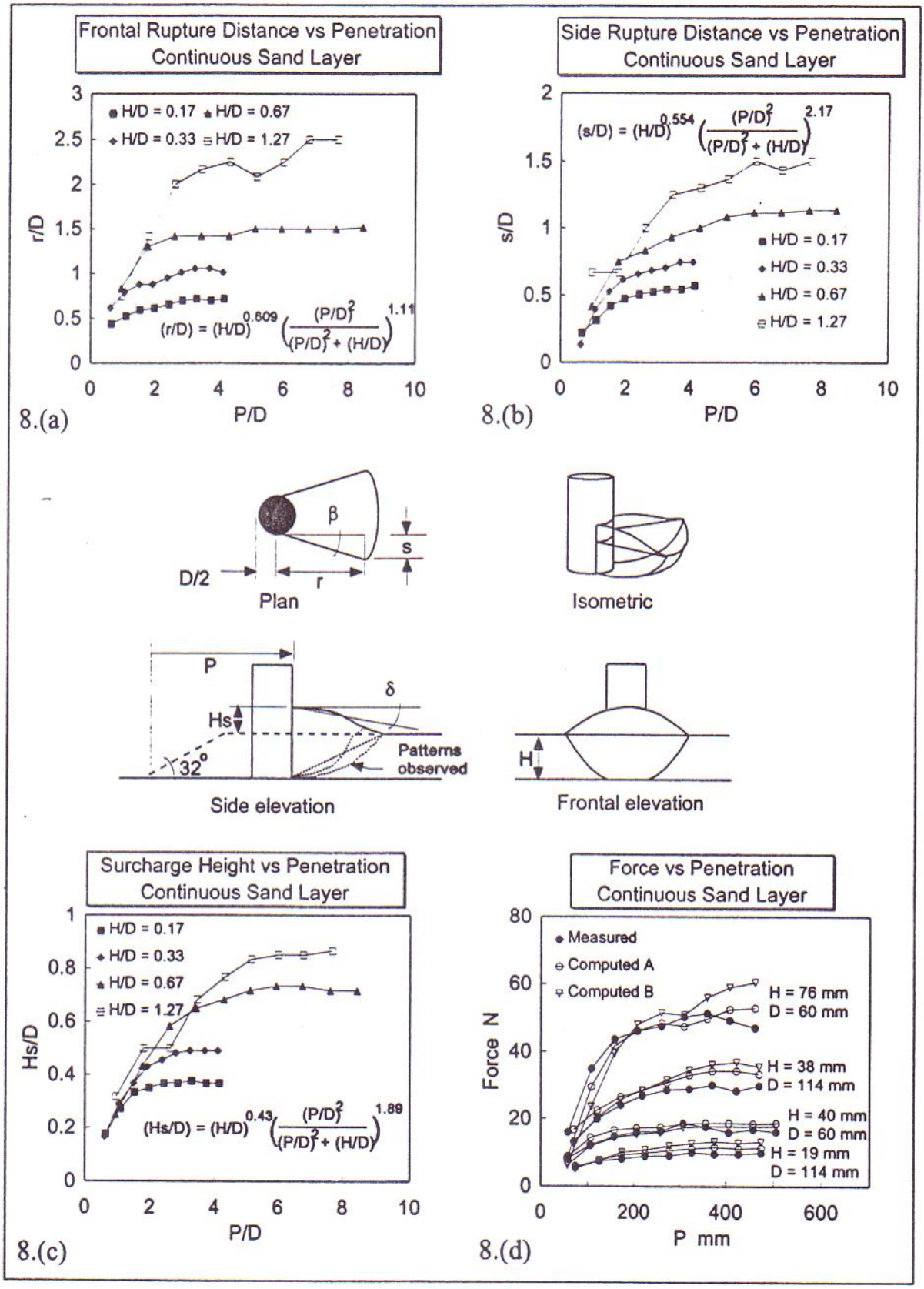
Frontal Rupture Distance vs Penetration
Continuous Sand Layer
H/D = 0.17
H/D = 0.33
H/D = 0.67
H/D = 1.27
r/D
P/D
(r/D) = (H/D)^0.609 ((P/D)^2 / ((P/D)^2 + (H/D)))^1.11
8.(a)
Side Rupture Distance vs Penetration
Continuous Sand Layer
(s/D) = (H/D)^0.554 ((P/D)^2 / ((P/D)^2 + (H/D)))^2.17
s/D
P/D
8.(b)
β
D/2
r
s
Plan
Isometric
P
Hs
δ
32°
Patterns observed
Side elevation
H
Frontal elevation
Surcharge Height vs Penetration
Continuous Sand Layer
Hs/D
P/D
(Hs/D) = (H/D)^0.43 ((P/D)^2 / ((P/D)^2 + (H/D)))^1.89
8.(c)
Force vs Penetration
Continuous Sand Layer
Measured
Computed A
Computed B
H = 76 mm
D = 60 mm
H = 38 mm
D = 114 mm
H = 40 mm
D = 60 mm
H = 19 mm
D = 114 mm
Force N
P mm
8.(d)

FIGURE 8.